G_{E_p}/G_{M_p} Ratio by Polarization Transfer in $\vec{e}p \rightarrow e\vec{p}$

M. K. Jones,[1] K. A. Aniol,[7] F. T. Baker,[4] J. Berthot,[6] P. Y. Bertin,[6] W. Bertozzi,[22] A. Besson,[6] L. Bimbot,[26] W. U. Boeglin,[10] E. J. Brash,[5] D. Brown,[21] J. R. Calarco,[23] L. S. Cardman,[30] C.-C. Chang,[21] J.-P. Chen,[30] E. Chudakov,[30] S. Churchwell,[8] E. Cisbani,[15] D. S. Dale,[18] R. De Leo,[14] A. Deur,[6,30] B. Diederich,[25] J. J. Domingo,[30] M. B. Epstein,[7] L. A. Ewell,[21] K. G. Fissum,[22] A. Fleck,[5] H. Fonvieille,[6] S. Frullani,[15] J. Gao,[22] F. Garibaldi,[15] A. Gasparian,[13,18] G. Gerstner,[1] S. Gilad,[22] R. Gilman,[2,30] A. Glamazdin,[19] C. Glashausser,[2] J. Gomez,[30] V. Gorbenko,[19] A. Green,[33] J.-O. Hansen,[30] C. R. Howell,[8] G. M. Huber,[5] M. Iodice,[15] C. W. de Jager,[30] S. Jaminion,[6] X. Jiang,[2] W. Kahl,[28] J. J. Kelly,[21] M. Khayat,[17] L. H. Kramer,[10] G. Kumbartzki,[2] M. Kuss,[30] E. Lakuriki,[29] G. Lavessière,[6] J. J. LeRose,[30] M. Liang,[30] R. A. Lindgren,[32] N. Liyanage,[22] G. J. Lolos,[5] R. Macri,[8] R. Madey,[17] S. Malov,[2] D. J. Margaziotis,[7] P. Markowitz,[10] K. McCormick,[25] J. I. McIntyre,[2] R. L. J. van der Meer,[5] R. Michaels,[30] B. D. Milbrath,[9] J. Y. Mougey,[12] S. K. Nanda,[30] E. A. J. M. Offermann,[30] Z. Papandreou,[5] C. F. Perdrisat,[1] G. G. Petratos,[17] N. M. Piskunov,[16] R. I. Pomatsalyuk,[19] D. L. Prout,[17] V. Punjabi,[3] G. Quéméner,[1,12] R. D. Ransome,[2] B. A. Raue,[10] Y. Roblin,[6] R. Roche,[11] G. Rutledge,[1] P. M. Rutt,[30] A. Saha,[30] T. Saito,[31] A. J. Sarty,[11] T. P. Smith,[23] P. Sorokin,[19] S. Strauch,[2] R. Suleiman,[17] K. Takahashi,[31] J. A. Templon,[4] L. Todor,[25] P. E. Ulmer,[25] G. M. Urciuoli,[15] P. Vernin,[27] B. Vlahovic,[24] H. Voskanyan,[34] K. Wijesooriya,[1] B. B. Wojtsekhowski,[30] R. J. Woo,[20] F. Xiong,[22] G. D. Zainea,[5] and Z.-L. Zhou[22]

(The Jefferson Lab Hall A Collaboration)

[1]*College of William and Mary, Williamsburg, Virginia 23187*
[2]*Rutgers, The State University of New Jersey, Piscataway, New Jersey 08855*
[3]*Norfolk State University, Norfolk, Virginia 23504*
[4]*University of Georgia, Athens, Georgia 30602*
[5]*University of Regina, Regina, SK S4S OA2, Canada*
[6]*Université Blaise Pascal/CNRS-IN2P3, F-63177 Aubière, France*
[7]*California State University at Los Angeles, Los Angeles, California 90032*
[8]*Duke University and TUNL, Durham, North Carolina 27708*
[9]*Eastern Kentucky University, Richmond, Kentucky 40475*
[10]*Florida International University, Miami, Florida 33199*
[11]*Florida State University, Tallahassee, Florida 32306*
[12]*Institut des Sciences Nucléaires, CNRS-IN2P3, F-38026 Grenoble, France*
[13]*Hampton University, Hampton, Virginia 23668*
[14]*INFN, Sezione di Bari and University of Bari, 70126 Bari, Italy*
[15]*INFN, Sezione Sanità and Istituto Superiore di Sanità, 00161 Rome, Italy*
[16]*JINR-LHE, 141980 Dubna, Moscow Region, Russian Federation*
[17]*Kent State University, Kent, Ohio 44242*
[18]*University of Kentucky, Lexington, Kentucky 40506*
[19]*Kharkov Institute of Physics and Technology, Kharkov, 310108, Ukraine*
[20]*University of Manitoba, Winnipeg, MB R3T 2N2, Canada*
[21]*University of Maryland, College Park, Maryland 20742*
[22]*Massachusetts Institute of Technology, Cambridge, Massachusetts 02139*
[23]*University of New Hampshire, Durham, New Hampshire 03824*
[24]*North Carolina Central University, Durham, North Carolina 27707*
[25]*Old Dominion University, Norfolk, Virginia 23508*
[26]*Institut de Physique Nucléaire, F-91406 Orsay, France*
[27]*CEA Saclay, F-91191 Gif-sur-Yvette, France*
[28]*Syracuse University, Syracuse, New York 13244*
[29]*Temple University, Philadelphia, Pennsylvania 19122*
[30]*Thomas Jefferson National Accelerator Facility, Newport News, Virginia 23606*
[31]*Tohoku University, Sendai 980, Japan*
[32]*University of Virginia, Charlottesville, Virginia 22901*
[33]*Western Cape University, Capetown, South Africa*
[34]*Yerevan Physics Institute, Yerevan 375036, Armenia*

The ratio of the proton's elastic electromagnetic form factors, G_{E_p}/G_{M_p}, was obtained by measuring P_t and P_ℓ, the transverse and the longitudinal recoil proton polarization, respectively. For elastic $\vec{e}p \rightarrow e\vec{p}$, G_{E_p}/G_{M_p} is proportional to P_t/P_ℓ. Simultaneous measurement of P_t and P_ℓ in a polarimeter provides good control of the systematic uncertainty. The results for the ratio G_{E_p}/G_{M_p} show a systematic decrease

as Q^2 increases from 0.5 to 3.5 GeV^2, indicating for the first time a definite difference in the spatial distribution of charge and magnetization currents in the proton.

PACS numbers: 25.30.Bf, 13.40.Gp, 14.20.Dh, 24.70.+s

Understanding the structure of the nucleon is of fundamental importance in nuclear and particle physics; ultimately such an understanding is necessary to describe the strong force. Certainly, for any QCD-based theory, its ability to predict the pion and nucleon form factors correctly is one of the most stringent tests of its validity, and hence precise data are required. The electromagnetic interaction provides a unique tool to investigate the structure of the nucleon. The elastic electromagnetic form factors of the nucleon characterize its internal structure; they are connected to its spatial charge and current distributions.

The earliest investigations of the proton form factor by Chambers and Hofstadter [1] established the dominance of the one-photon exchange process in the elastic ep reaction. It indicated that the Dirac, F_{1_p}, and Pauli, F_{2_p}, form factors depend only on four-momentum transfer squared which for elastic scattering is in the spacelike region. F_{1_p} and F_{2_p} were found to have approximately the same Q^2 dependence up to ≈ 0.5 GeV^2, where $Q^2 = 4E_e E'_e \sin^2 \frac{\theta_e}{2}$, E'_2 and θ_e are the scattered electron's energy and angle, respectively, and E_e is the incident beam energy. The data were fitted with a dipole shape, $G_D = (1 + \frac{Q^2}{0.71})^{-2}$, characteristic of an exponential radial distribution.

The elastic ep cross section can be written in terms of the electric, $G_{E_p}(Q^2)$, and magnetic, $G_{M_p}(Q^2)$, Sachs form factors, which are defined as

$$G_{E_p} = F_{1_p} - \tau \kappa_p F_{2_p} \quad \text{and} \quad G_{M_p} = F_{1_p} + \kappa_p F_{2_p}, \tag{1}$$

where $\tau = Q^2/4M^2$, κ_p is the anomalous nucleon magnetic moment, and M is the mass of the proton. In the limit $Q^2 \to 0$, $G_{E_p} = 1$ and $G_{M_p} = \mu_p$, the proton magnetic moment. The unpolarized ep cross section is

$$\frac{d\sigma}{d\Omega} = \frac{\alpha^2 E'_e \cos^2 \frac{\theta_e}{2}}{4E_e^3 \sin^4 \frac{\theta_e}{2}} \left[G_{E_p}^2 + \frac{\tau}{\epsilon} G_{M_p}^2 \right] \left(\frac{1}{1 + \tau} \right), \tag{2}$$

where ϵ is the virtual photon longitudinal polarization, $\epsilon = [1 + 2(1 + \tau) \tan^2(\frac{\theta_e}{2})]^{-1}$.

In the Rosenbluth method [2], the separation of $G_{E_p}^2$ and $G_{M_p}^2$ is achieved by measuring the cross section at a given Q^2 over a range of ϵ values that are obtained by changing the beam energy and scattered electron angle. In Eq. (2) the G_{M_p} part of the cross section is multiplied by τ; therefore, as Q^2 increases, the cross section becomes dominated by G_{M_p}, making the extraction of G_{E_p} more difficult. Figure 1 shows measurements of proton form factors obtained by using this method. For $Q^2 < 1$ GeV^2, the uncertainties in both G_{E_p} and G_{M_p} are only a few percent, and one finds that $G_{M_p}/\mu_p G_D \simeq G_{E_p}/G_D \simeq 1$. For G_{E_p} above $Q^2 = 1$ GeV^2, the large uncertainties and the divergence in results between different experiments, as

seen in Fig. 1a, illustrate the difficulties in obtaining G_{E_p} by the Rosenbluth method. In contrast, the uncertainties on G_{M_p} remain small up to $Q^2 = 31.2$ GeV^2 [10].

The combination of high energy, current, and polarization, unique to the Continuous Electron Beam Accelerator Facility of the Jefferson Laboratory (JLab), makes it possible to investigate the internal structure of the nucleon with higher precision and different experimental techniques. This experiment used the powerful technique of polarization transfer. For one-photon exchange, the scattering of longitudinally polarized electrons results in a transfer of polarization to the recoil proton with only two nonzero components, P_t perpendicular to, and P_ℓ parallel to the proton momentum in the scattering plane, given by [11]

$$I_0 P_t = -2\sqrt{\tau(1 + \tau)} G_{E_p} G_{M_p} \tan \frac{\theta_e}{2}, \tag{3}$$

$$I_0 P_\ell = \frac{1}{M} (E_e + E_{e'}) \sqrt{\tau(1 + \tau)} G_{M_p}^2 \tan^2 \frac{\theta_2}{2}, \tag{4}$$

where $I_0 = G_{E_p}^2 + \frac{\tau}{\epsilon} G_{M_p}^2$. Equations (3) and (4) together give

$$\frac{G_{E_p}}{G_{M_p}} = -\frac{P_t}{P_\ell} \frac{(E_e + E_{e'})}{2M} \tan\left(\frac{\theta_e}{2}\right). \tag{5}$$

The ratio G_{E_p}/G_{M_p} is obtained from a simultaneous measurement of the two recoil polarization components in the
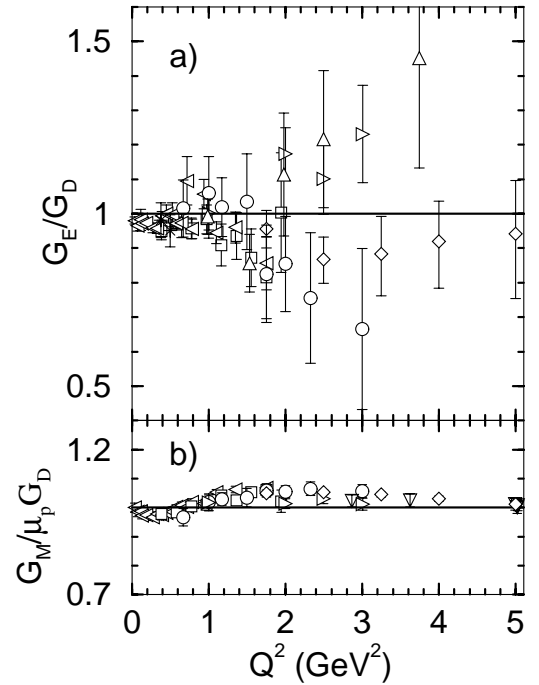

FIG. 1. World data for (a) G_{E_p}/G_D and (b) $G_{M_p}/\mu_p G_D$. References [3] (Δ), [4] ($\square$), [5] ($\triangleleft$), [6] ($\bigcirc$), [7] ($\triangleright$), [8] ($\diamond$), [9] ($*$), and [10] (∇) versus Q^2.

polarimeter. Neither the beam polarization nor the polarimeter analyzing power needs to be known, which results in small systematic uncertainties. This method was first used recently by Milbrath *et al.* [9] at MIT-Bates to measure the ratio G_{E_p}/G_{M_p} at low Q^2.

Our experiment was done in Hall A at JLab. Longitudinally polarized electron beams with energies between 0.934 and 4.090 GeV were scattered in a 15-cm-long circulating liquid hydrogen (LH_2) target, refrigerated to 19 K. The kinematic settings are given in Table I. For the four highest Q^2 points, a bulk GaAs photocathode, excited by circularly polarized laser light, produced beams with ~0.39 polarization and currents up to ~115 μA; the helicity was flipped at 30 Hz. For the lower Q^2 points, a strained GaAs crystal was used, and typical polarizations of ~0.60 were achieved with currents up to ~15 μA; the helicity was flipped at 1 Hz. The beam polarization was measured with a Mott polarimeter in the injector line and with a Møller polarimeter in Hall A [12].

Elastic *ep* events were selected by detecting the scattered electrons and protons in coincidence in the two identical high resolution spectrometers (HRS) of Hall A [12]. The HRS deflect particles vertically by 45° and accept a maximum central trajectory momentum of 4 GeV/c with a 6.5 msr angular acceptance, ±5% momentum acceptance, and ~10^{-4} momentum resolution. The two vertical drift chambers installed close to the focal plane of each HRS give precise reconstruction of the positions and angles at the target. The trigger was defined by a coincidence between the signals from two scintillator planes in each of the two HRS. A focal plane polarimeter (FPP) was installed in the hadron HRS. In the FPP, two front straw chambers define the incident proton trajectory and two rear straw chambers define the proton trajectory after scattering in the graphite analyzer [13]. The graphite analyzer consists of five sets of graphite plates which can be moved out to collect straight-through trajectories for alignment of the FPP chambers. Graphite thicknesses between 11 and 50 cm were used in order to optimize the FPP figure of merit.

TABLE I. The ratio $\mu_p G_{E_p}/G_{M_p} \pm$ statistical uncertainty (1σ). Δ_{syst} is the systematic uncertainty. ΔQ^2 is half the Q^2 acceptance. $\langle\chi\rangle$ is the average spin precision angle.

$\langle Q^2\rangle \pm \Delta Q^2$ (GeV^2)	E_e (GeV)	$\langle\chi\rangle$ (deg)	$\mu_p G_{E_p}/G_{M_p}$ ($\pm$ stat. uncert.)	Δ_{syst}
0.49 ± 0.04	0.934	105	0.966 ± 0.022	0.011
0.79 ± 0.02	0.934	118	0.950 ± 0.015	0.017
1.18 ± 0.07	1.821	136	0.869 ± 0.014	0.027
1.48 ± 0.11	3.395	150	0.798 ± 0.033	0.035
1.77 ± 0.12	3.395	164	0.728 ± 0.026	0.047
1.88 ± 0.13	4.087	168	0.720 ± 0.031	0.060
2.47 ± 0.17	4.090	196	0.726 ± 0.027	0.062
2.97 ± 0.20	4.087	218	0.612 ± 0.032	0.056
3.47 ± 0.20	4.090	239	0.609 ± 0.047	0.045

The azimuthal angular distribution after a second scattering in the analyzer of the FPP is given by

$$N_p(\vartheta, \varphi) = N_p(\vartheta)\{1 + [hA_c(\vartheta)P_t^{\text{FPP}} + \alpha]\sin\varphi \\ - [hA_c(\vartheta)P_n^{\text{FPP}} + \beta]\cos\varphi\}, \quad (6)$$

where h is the electron beam polarization, $N_p(\vartheta)$ is the number of protons scattered in the polarimeter, ϑ and φ are the polar and azimuthal angles after scattering, and $A_c(\vartheta)$ is the analyzing power; P_t^{FPP} and P_n^{FPP} are the in-plane polarization components, transverse and normal, respectively, at the FPP analyzer. Instrumental asymmetries (α and β) are canceled by taking the difference of the azimuthal distributions for positive and negative electron beam helicity. Fourier analysis of this difference distribution gives $hA_c(\vartheta)P_t^{\text{FPP}}$ and $hA_c(\vartheta)P_n^{\text{FPP}}$.

The proton spin precesses in the fields of the magnetic elements of the HRS, and therefore the polarizations at the target and the FPP are different; they are related through a spin transport matrix $\mathbf{P}^{\text{FPP}} = (\mathbf{S}) \times \mathbf{P}$, where $\mathbf{P}^{\text{FPP}}$ and $\mathbf{P}$ are polarization column vectors (n, t, ℓ) at the FPP and target, respectively, and $(\mathbf{S})$ is the spin transport matrix. A novel method was developed to extract the values of the polarization components P_t and P_ℓ at the target from the FPP azimuthal distribution; the integrals in the Fourier analysis were replaced with sums weighted by the values of the matrix elements, S_{ij}, of each event [14]. The matrix elements S_{ij} depend upon the angular (θ and ϕ) and spatial (y) coordinates at the target and proton momentum (p). The S_{ij}'s were calculated for each event from the reconstructed θ, ϕ, y, p using the spin matrix determined by a magnetic transport code. Both the ray-tracing code SNAKE [15] and the differential-algebra-based code COSY [16] were used, and the spin precession corrections from both methods agree within experimental uncertainties. The stability of the method was studied in detail for all Q^2. The data were analyzed in bins of each one of the four target variables, one at a time. The results showed that the extracted G_{E_p}/G_{M_p} ratio is independent of each of these variables.

The results for the ratio $\mu_p G_{E_p}/G_{M_p}$ are shown as filled circles in Fig. 2a, and as the ratio $Q^2 F_2/F_1$, obtained from Eq. (1), in Fig. 2b; in both figures only the statistical uncertainties are plotted as error bars. The data are tabulated in Table I, where both statistical and systematic uncertainties are given for each data point. Three sources contribute to the systematic uncertainty: measurement of the target variables, positioning and field strength of the HRS magnetic elements, and uncertainties in the dipole fringe-field characterization. The systematic uncertainties would shift all data points in the same direction, either up or down. No radiative correction has been applied to the results. External radiative effects are canceled by switching the beam helicity. The internal correction is due to hard photon emission, two-photon exchange, and higher-order contributions. A dedicated calculation [17] predicts the first to be of the order of a few percent. Preliminary indications
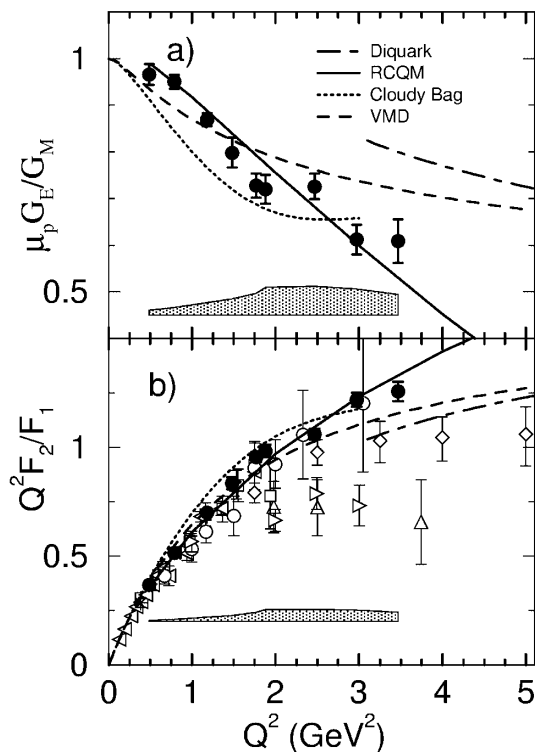
FIG. 2. (a) The ratio $\mu_p G_{E_p}/G_{M_p}$ from this experiment, compared with theoretical calculations. (b) The ratio $Q^2 F_{2_p}/F_{1_p}$ for the same data, compared to the same theoretical models as in (a) and world data; symbols as in Fig. 1. In both (a) and (b) the absolute value of systematic error from this experiment is shown by the shaded area.

are that the two other contributions are also at the same percentage level.

The most important feature of the data is the sharp decline of the ratio $\mu_p G_{E_p}/G_{M_p}$ as Q^2 increases, which indicates that G_{E_p} falls faster than G_{M_p}. Furthermore, as $G_{M_p}/\mu_p G_D$ is approximately constant, it follows that G_{E_p} falls more rapidly with Q^2 than the dipole form factor G_D.

Results from this experiment are consistent with the earlier results of Refs. [4–6] which have much larger uncertainties. Our results are compatible with the SLAC data of Ref. [8] up to about Q^2 of 2.5 GeV^2, considering the larger uncertainties, but our results are in definite disagreement with the older results of Ref. [7] from SLAC, as seen in Fig. 2b.

The $Q^2 F_2/F_1$ ratio shown in Fig. 2b indicates a continuing increase with Q^2, contradicting earlier observations based on the data of Refs. [7,8] that it might have reached a constant value as predicted in perturbative QCD (pQCD): $F_1 \sim \frac{1}{Q^4}$ and $F_2 \sim \frac{1}{Q^6}$ [18]. It would be of great interest to explore the larger Q^2 region where pQCD will dominate. Extension of this experiment to larger Q^2 has become a very interesting prospect and is planned in the near future.

So far, all theoretical models of the nucleon form factors are based on effective theories; they all rely on a comparison with existing data and their parameters

are adjustable. Much work has been done with the goal of bridging the low and high Q^2 regimes. There are two quite different approaches to calculate nucleon form factors. In the first approach, the mesonic degrees of freedom are explicit, as in calculations based on vector meson dominance (VMD) [19–22], models comprising a three-quark core dressed with pseudoscalar mesons [23], and a calculation based on the solitonic nature of the nucleon [24]. The second approach consists of QCD-based quark models; these include models such as relativistic constituent quark (RCQM) [25–27], diquark [28], cloudy bag [29], and QCD sum rule [30]. Calculations of the nucleon form factors from lattice QCD are in progress [31].

In Fig. 2, we show as a dashed curve the ratios of $\mu_p G_{E_p}/G_{M_p}$ and $Q^2 F_{2_p}/F_{1_p}$ calculated from the latest published fit to the proton and neutron form factors of Mergell et al. [22] based on VMD (not including data from this experiment). These authors use dispersion relations for the form factors, with spectral functions taking into account the dominant vector meson poles as well as the two-pion channel; an asymptotic behavior consistent with pQCD was also included.

In the earliest study of the RCQM, Chung and Coester [25] investigated the effect of the constituent quark masses, the anomalous magnetic moment of the quarks, F_{2q}, and the confinement scale parameter. Recently Coester introduced a form factor for F_{2q} to reproduce the present data; the result is the solid curve in Fig. 2 [26]. This illustrates how the new G_{E_p}/G_{M_p} data can help constrain the basic inputs to a particular model. The dashed-dotted curve in Fig. 2 shows the recently reevaluated diquark model prediction of Kroll et al. [28]. In the limit $Q^2 \to \infty$ this model is equivalent to the hard-scattering formulation of pQCD. Calculations based on the cloudy bag model predict the right slope for G_{E_p}/G_{M_p} shown as a dotted curve in Fig. 2; this model includes an elementary pion field coupled to the quarks inside the bag such that chiral symmetry is restored [29].

Recent theoretical developments indicate that measurements of the elastic form factors of the proton to large Q^2 may shed light on the problem of nucleon spin. This connection between elastic form factors and spin has been demonstrated within the skewed parton distribution (SPD) formalism by Ji [32]. The first moment of the SPD taken in the forward limit yields, according to the angular momentum sum rule [32], a contribution to the nucleon spin from the quarks and gluons, including the orbital angular momentum. By subsequently applying the sum rule to the SPD, it should become possible to estimate the total contribution of the valence quarks to the proton spin [33,34].

In conclusion, we have presented a new measurement of G_{E_p}/G_{M_p} obtained in a polarization transfer experiment with unprecedented accuracy. The results demonstrate for the first time that the Q^2 dependence of G_{E_p} and G_{M_p} is significantly different. The quality of the JLab data will place a tight constraint on the theoretical models. Results

———————

[1] E. E. Chambers and R. Hofstadter, Phys. Rev. **103**, 1454 (1956).
[2] M. N. Rosenbluth, Phys. Rev. **79**, 615 (1950).
[3] J. Litt *et al.,* Phys. Lett. **31B**, 40 (1970).
[4] Ch. Berger *et al.,* Phys. Lett. **35B**, 87 (1971).
[5] L. E. Price *et al.,* Phys. Rev. D **4**, 45 (1971).
[6] W. Bartel *et al.,* Nucl. Phys. **B58**, 429 (1973).
[7] R. C. Walker *et al.,* Phys. Rev. D **49**, 5671 (1994).
[8] L. Andivahis *et al.,* Phys. Rev. D **50**, 5491 (1994).
[9] B. Milbrath *et al.,* Phys. Rev. Lett. **80**, 452 (1998); Phys. Rev. Lett. **82**, 2221(E) (1999).
[10] A. F. Sill *et al.,* Phys. Rev. D **48**, 29 (1993).
[11] A. I. Akhiezer and M. P. Rekalo, Sov. J. Part. Nucl. **3**, 277 (1974); R. Arnold, C. Carlson, and F. Gross, Phys. Rev. C **23**, 363 (1981).
[12] http://www.jlab.org/Hall-A/equipment/
[13] M. K. Jones *et al.,* in *Intersections Between Particle and Nuclear Physics,* edited by T. W. Donnelly, AIP Conf. Proc. No. 412 (AIP, New York, 1997), p. 342; http://www.jlab.org/Hall-A/equipment/detectors/fpp_overview.html
[14] G. Quéméner *et al.,* Nucl. Phys. **A654**, 543c (1999).
[15] P. Vernin, SNAKE (private communication), SPhN-CEA in Saclay, France.
[16] M. Bertz, COSY INFINITY version 7, Michigan State University NSCL Technical Report MSUCL-977, 1995.
[17] A. V. Afanasev, I. Akushevich, and N. Merenkov (private communication).
[18] S. J. Brodsky and G. R. Farrar, Phys. Rev. D **11**, 1309 (1975).
[19] G. Höhler *et al.,* Nucl. Phys. **B114**, 505 (1976).
[20] F. Iachello, A. D. Jackson, and A. Landé, Phys. Lett. **43B**, 191 (1973).
[21] M. F. Gari and W. Krümpelmann, Z. Phys. A **322**, 689 (1985).
[22] P. Mergell, U. G. Meissner, and D. Drechsel, Nucl. Phys. **A596**, 367 (1996).
[23] Z. Dziembowski *et al.,* Ann. Phys. (N.Y.) **258**, 1 (1997).
[24] G. Holzwarth, Z. Phys. A **356**, 339 (1996).
[25] P. L. Chung and F. Coester, Phys. Rev. D **44**, 229 (1991).
[26] F. Coester (private communication).
[27] I. G. Aznauryan, Phys. Lett. B **316**, 391 (1993).
[28] P. Kroll, M. Schürmann, and W. Schweiger, Z. Phys. A **338**, 339 (1991); (private communication).
[29] D. H. Lu, A. W. Thomas, and A. G. Williams, Phys. Rev. C **57**, 2628 (1998); D. H. Lu, S. N. Yang, and A. W. Thomas, Report ADP 99-36/t373.
[30] A. V. Radyushkin, Acta Phys. Pol. B **15**, 40 (1984).
[31] S. Capitani *et al.,* Nucl. Phys. (Proc. Suppl.) **B73**, 294 (1999).
[32] X. Ji, Phys. Rev. D **55**, 7114 (1997); Phys. Rev. Lett. **78**, 610 (1997).
[33] A. V. Radyushkin, JLab-THY-98-10, hep-ph/9803316.
[34] A. V. Afanasev, in Proceedings of the INT/JLab Workshop, Newport News, 1999, edited by C. Carlson and A. Radyushkin (to be published) (hep-ph/9910565).